Plasma Sources Science and Technology

PAPER

Extended scaling and Paschen law for micro-sized radiofrequency plasma breakdown

To cite this article: Min Uk Lee *et al* 2017 *Plasma Sources Sci. Technol.* **26** 034003

IOP Publishing Plasma Sources Science and Technology
Plasma Sources Sci. Technol. **26** (2017) 059502 (1pp) https://doi.org/10.1088/1361-6595/aa6771

Corrigendum: Extended scaling and Paschen law for micro-sized radiofrequency plasma breakdown (2017 *Plasma Sources Sci. Technol.* 26 034003)

Min Uk Lee[1], Jimo Lee[1], Jae Koo Lee[1] and Gunsu S Yun[1,2,3]

[1] Division of Advanced Nuclear Engineering, Pohang University of Science and Technology, Pohang 37673, Republic of Korea
[2] Department of Physics, Pohang University of Science and Technology, Pohang 37673, Republic of Korea
[3] Center for Attosecond Science, Max Planck POSTECH/Korea Research Initiative (MPK), Pohang 37673, Republic of Korea

E-mail: jkl@postech.ac.kr and gunsu@postech.ac.kr

Received 10 March 2017
Accepted for publication 17 March 2017
Published 5 April 2017

Typographical errors in the definitions of the diffusion coefficients and the mobility at the unit gas pressure used in equation (22) on page 5 should be corrected as follows: $D_{\mathrm{T}0} = pD_{\mathrm{T}}$, $D_{\mathrm{L}0} = pD_{\mathrm{L}}$, and $\mu_{e0} = p\mu_e$.

IOP Publishing Plasma Sources Science and Technology

Plasma Sources Sci. Technol. **26** (2017) 034003 (7pp) https://doi.org/10.1088/1361-6595/aa52a8

Extended scaling and Paschen law for micro-sized radiofrequency plasma breakdown

Min Uk Lee[1], Jimo Lee[1], Jae Koo Lee[1,4] and Gunsu S Yun[1,2,3,4]

[1] Division of Advanced Nuclear Engineering, Pohang University of Science and Technology, Pohang 37673, Republic of Korea
[2] Department of Physics, Pohang University of Science and Technology, Pohang 37673, Republic of Korea
[3] Center for Attosecond Science, Max Planck POSTECH/Korea Research Initiative (MPK), Pohang 37673, Republic of Korea

E-mail: jkl@postech.ac.kr and gunsu@postech.ac.kr

Received 29 July 2016, revised 7 November 2016
Accepted for publication 8 December 2016
Published 10 February 2017

Abstract

The single particle motion analysis and particle-in-cell merged with Monte Carlo collision (PIC/MCC) simulations are compared to explain substantial breakdown voltage reduction for helium microwave discharge above a critical frequency corresponding to the transition from the drift-dominant to the diffusion-dominant electron loss regime. The single particle analysis suggests that the transition frequency is proportional to the product of p^{-m} and $d^{-(m+1)}$ where p is the neutral gas pressure, d is the gap distance, and m is a numerical parameter, which is confirmed by the PIC simulation. In the low-frequency or drift-dominant regime, i.e., γ-regime, the secondary electron emission induced by ion drift motion is the key parameter for determining the breakdown voltage. The fluid analysis including the secondary emission coefficient, γ, induces the extended Paschen law that implies the breakdown voltage is determined by pd, f/p, γ, and d/R where f is the frequency of the radio or microwave frequency source, and R is the diameter of electrode. The extended Paschen law reproduces the same scaling law for the transition frequency and is confirmed by the independent PIC and fluid simulations.

Keywords: microplasma, breakdown, transition, scaling, Paschen's law, PIC simulation, fluid simulation

(Some figures may appear in colour only in the online journal)

1. Introduction

Both basic and applied researches in the atmospheric cold plasmas have grown exponentially in the past two decades [1]. There exist numerous operating sources and many different forms of discharge devices including DC [2], pulsed [3], RF [4, 5], microwave [6, 7], and dual frequency [8]. Recently, applications using microwave frequency source are emerging due to several advantages such as higher electron temperature and higher density of radical species [1, 7, 9, 10], particularly in biomedical area.

There has been considerable research on the gas breakdown mechanism and validity of the Paschen law for a wide range of driving frequencies [11–14] and gap distances [15, 16]. Such fundamental research is essential because understanding of the breakdown process at different conditions is useful not only for development of efficient plasma source devices but also for controlling the plasma parameters in individual applications. For example, in numerical simulations and several experiments [14, 17–20] for various discharge conditions, abrupt transitions in the breakdown voltage have been observed (see figure 1), implying the shift of breakdown mechanism.

In this paper, we propose that the abrupt transition corresponds to the transition from the so-called γ-regime [21] to

[4] Authors to whom any correspondence should be addressed.

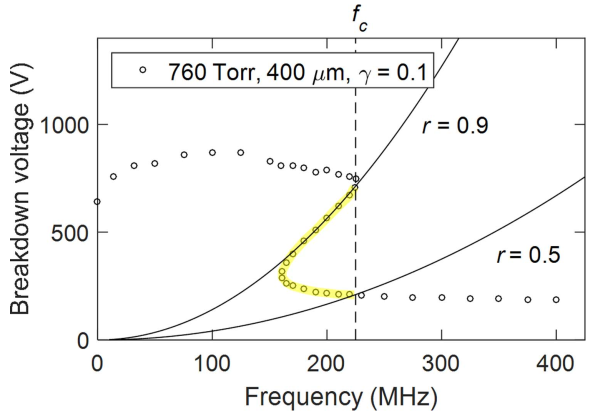

Figure 1. The PIC simulation results of breakdown voltages for atmospheric pressure He discharge between planar electrodes with the gap distance of 400 μm, showing a typical 'Z' shape dependence on the driving frequency. The breakdown voltage changes drastically at the critical frequency f_c indicated by the dashed line. The transition region is bounded by the two solid lines obtained from the single particle analysis corresponding to $r = 0.5$ and $r = 0.9$, respectively.

α-regime [22]. In the γ-regime, the secondary emission is the key source of electrons for discharge sustainment because of large electron-drift wall loss driven by the electric field. In the α-regime, however, the breakdown rarely depends on the secondary emission. At critical condition (determined by gap distance, pressure, and/or driving frequency), the electron drift amplitude, which is defined as the amplitude of oscillating electrons forced by high-frequency electric field, becomes smaller than the electrode gap and the electron wall loss is minimized. This improved confinement of electrons is responsible for the breakdown voltage reduction.

This conjecture is verified by the single particle analysis and is also corroborated by the particle-in-cell simulations merged with Monte Carlo collision (PIC/MCC) [23, 24]. In particular, the scaling law, which describes the relation among the transition frequency, gap distance, and neutral gas pressure, is derived from the single particle analysis and confirmed by the PIC simulations. Furthermore, the dependence of the breakdown voltage on these parameters is analyzed using fluid equations under the drift-diffusion approximation [13, 14]. The fluid analysis yields an extended Paschen law which represents the breakdown voltage as a function of not only the neutral gas pressure and gap distance but also the driving frequency and geometry of electrodes incorporating the secondary emissions for γ-regime and the same scaling law as a corollary. The extended Paschen law is validated by the PIC and fluid simulations [25, 26].

2. Scaling law for transition frequency

The abrupt breakdown voltage transition is observed in the PIC simulations as illustrated in figure 1, showing a typical 'Z' transition of the breakdown voltage on the driving frequency. The numerical parameters and simulation conditions used to ensure the reliable results are detailed in [20]. The transition frequency f_c is defined as the right-most extremum in the 'Z' shape breakdown curve. The single particle analysis to be explained below in detail shows that the transition region (highlighted in figure 1) corresponds to a certain range of the amplitude of electron drift motion (Δx) normalized by the electrode gap distance d, $r = \Delta x/d$.

To describe the transition mechanism, let us consider the kinetic single particle motion along the RF field line which is perpendicular to the electrodes,

$$m_e \frac{\mathrm{d}v_e}{\mathrm{d}t} = eE_{\mathrm{rf}} \cos 2\pi ft - m_e v_e \nu_m, \tag{1}$$

where m_{e} is the electron density, v_{e} is the electron drift velocity relative to the neutral gas particles, e is the electron charge, E_{rf} is the peak amplitude of RF electric field, and ν_{m} is the electron-neutral momentum collision frequency. If we neglect the space charge effect at the early stage of breakdown, $E_{\mathrm{rf}} = V_{\mathrm{rf}}/d$, where V_{rf} is the amplitude of the RF potential and d is the gap distance, then the electron motion can be written,

$$\frac{\mathrm{d}v_e}{\mathrm{d}t} = \frac{eV_{\mathrm{rf}}}{m_e d} \cos 2\pi ft - n_{\mathrm{g}} \sigma_{eg}(v_e)|v_e| v_e, \tag{2}$$

where n_{g} is the neutral gas density, $\sigma_{eg}(v_e)$ is the electron-neutral momentum collision cross section [27]. Note that the collision frequency $\nu_m = n_{\mathrm{g}}\sigma_{eg}(v_e)|v_e|$ is an ensemble average of elastic collisions of an electron (test particle) over the neutral gas particles (field particles). Let us consider the normalized single particle motion by multiplying $d/|v_{e0}|^2$ and equation (2) where v_{e0} is the characteristic velocity of the electron. Equation (2) becomes

$$\frac{\mathrm{d}}{|v_{e0}|} \frac{\mathrm{d}\hat{v}_e}{\mathrm{d}t} = \frac{eV_{\mathrm{rf}}}{m_e |v_{e0}|^2} \cos 2\pi \hat{f}\hat{t} - \hat{\lambda}^{-1} |\hat{v}_e| \hat{v}_e, \tag{3}$$

where the normalized velocity of the electron $\hat{v}_e = v_e/|v_{e0}|$, normalized frequency $\hat{f} = fd/v_{e0}$, normalized time $\hat{t} = tv_{e0}/d$, and normalized mean free path $\hat{\lambda} = [dn_{\mathrm{g}}\sigma_{eg}(\hat{v}_e)]^{-1}$.

In figure 1, the PIC simulation result is overlaid on the solid curve that indicates the critical boundary, where the contour line $r = 0.5$, at the transition frequency f_c. Contour line r is obtainable by solving equation (2) for V_{rf} with fixed d, n_{g}, and constant σ_{eg} (the latter condition is justifiable for non-Ramsauer gas like Helium). This implies that when the driving frequency decreases, the electron drift wall loss becomes large enough (i.e., $r > 0.5$) to cause transition between α- and γ-regimes. Owing to the fact that the single particle analysis does not consider the γ effect, the PIC simulations with different values of secondary emission coefficient between 0.01 to 1 have been performed to check any dependence of f_c on γ. The transition frequency decreases slightly for larger γ but the dependence is very weak; within 10% of the calculated f_c from the single particle analysis at $r = 0.5$. It is found that the extremum point of the breakdown curve corresponds to $r = 0.9$. Therefore, the breakdown curve may be divided into three separate regimes: γ, transition, and α. Each regime corresponds to $r > 0.9$, $0.5 < r < 0.9$, and $r < 0.5$, repectively.

The scaling law, which describes the relation among the transition frequency, gap distance, and neutral gas pressure,

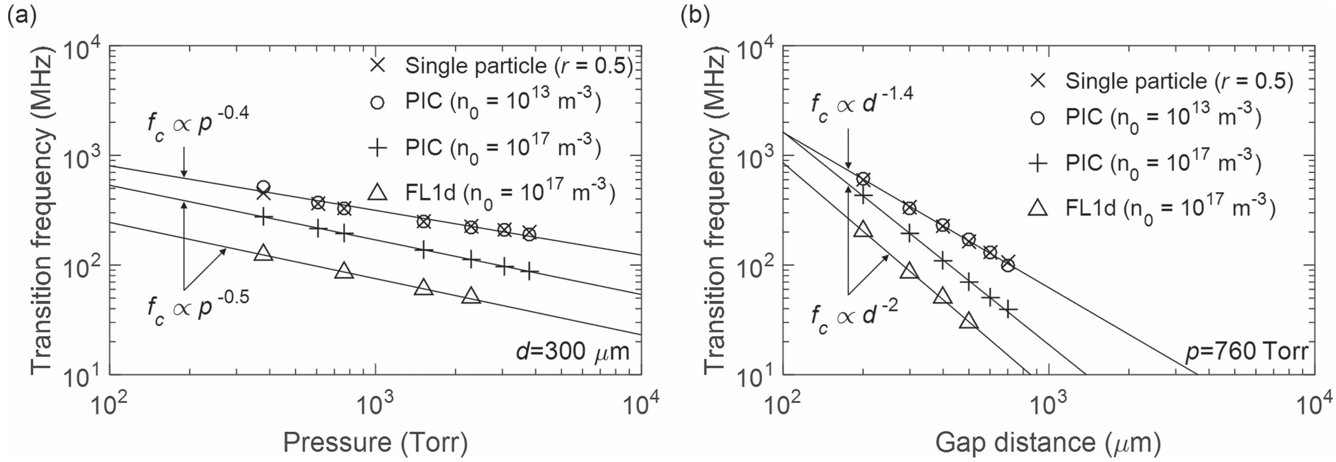

Figure 2. Transition frequency with respect to (a) neutral gas pressure at a fixed gap and (b) gap distance at a fixed pressure for different initial seed electron density n_0. Excellent agreement between the PIC and the single particle analysis is observed for low n_0.

has been checked by the PIC simulations as illustrated in figure 2 for a wide range of neutral gas pressure and different gap distances. Note that the previous simulation results [20] and the PIC results studied in this paper with different initial seed electron density conditions have different exponents of p and d. The deviation is caused by the space charge effect from the abundant initial seed electrons which shield the externally applied electric field with the self-consistent electric field creating better confinement for electrons, and thus it decreases the transition frequency.

It is also interesting to compare the PIC with the fluid simulation in figure 2. Using the fluid code FL1d [25], the simulaion results show the same slope as the PIC simulation results with the same n_0 of 10^{17} m^{-3}. However, the absolute values of the transition frequency in the fluid simulations are much lower than those in the PIC simulations. Similar discrepancies are often found between the FL1d and PIC but both simulations tend to have the same trend [25, 26]. Even at lower initial seed electron density, however, the scaling law derived from the kinetic analysis or the PIC is not observed in the fluid simulation. This implies that the fluid simulation cannot fully depict the kinetic nature of the gas breakdown [20]. The assumption of the Maxwellian electron energy distribution taken by the fluid simulation is presumably the main reason why the PIC and fluid simulation results show such divergences [23, 25].

The normalized electron drift amplitude r as a function of $\hat{f}$ and $\hat{\lambda}$ derived from the numerical solutions of equation (3) is shown as a contour plot in figure 3. The contour line $r = 0.5$ of figure 3 corresponds to the boundary of significant drift wall loss observed in figure 1, and the plasma regime shifts from α- to γ-regime below the contour line of $r = 0.5$ in figure 3 ($r > 0.5$). The scaling law for the transition frequency f_c can be obtained by approximating the transition boundary at $r = 0.5$ as $\hat{f}_c = \hat{\lambda}^m$, where m is a positive exponent. Transformation of this relation into a non-normalized form yields the desired scaling law for f_c:

$$f_c \propto p^{-m} d^{-(m+1)}, \tag{4}$$

where p is the neutral gas pressure and d is the gap distance.

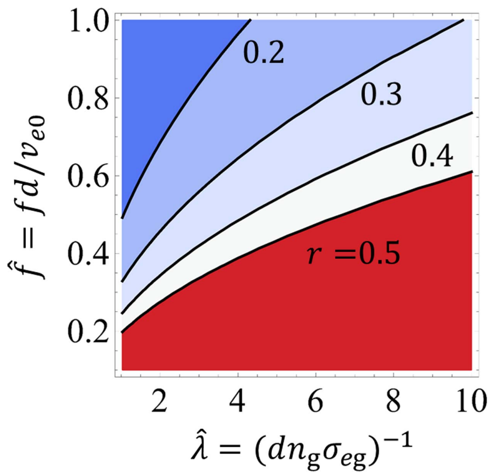

Figure 3. Normalized frequency against normalized mean free path. Contour lines indicate $r = \Delta x/d$, the ratio of the electron drift amplitude (Δx) over the gap distance (d).

This scaling law originated from the single particle analysis shows a good agreement with the PIC simulation results with $m = 0.4$ only when the initial seed electron density is low enough ($n_0 \leqslant 10^{13}$ m^{-3}) for minimal space charge effect.

3. Extended Paschen law for radiofrequency microplasmas

For DC discharge, the breakdown voltage can be expressed as a function of the product of the neutral gas pressure and gap distance, which is known as Paschen law. In the case of RF discharge, other factors such as f/p and d/R determine the breakdown voltage, where R is the radius of the electrode in a cylindrical discharge system [12, 14]. For radiofrequency microplasmas, however, the extended Paschen law with the ion bombardment induced secondary emission, ion-enhanced field emission, or field-enhanced thermionic emission dominant regimes has not been clearly investigated in the past.

In the transition and α-regime where the electron drift amplitude over gap distance r is below 0.9, the secondary

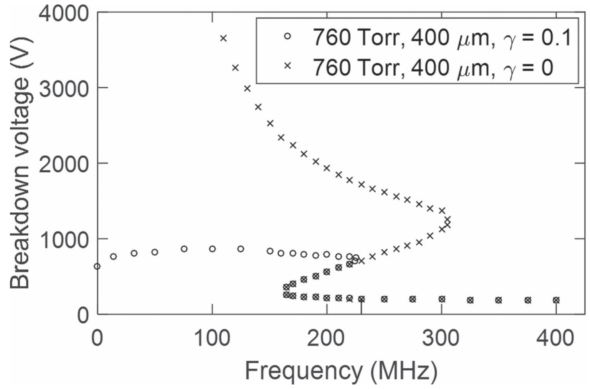

Figure 4. In the α-regime above the transition frequency, the breakdown voltage is rarely affected by the secondary electron emission coefficient γ. In the γ-regime below the transition frequency, the breakdown voltage significantly depends on the value of γ.

emission barely affects the breakdown voltage. In γ-regime ($r > 0.9$), however, the breakdown voltage strongly depends on the secondary emission coefficient induced by the ion bombardment due to the drift wall loss caused by high electric field (see figure 4). For the fluid analysis, we simultaneously consider the ion and electron density continuity equations including the secondary emission, field emission, and thermionic emission.

Because drift wall loss becomes more dominant than diffusion loss in γ-regime, the continuity equation of ion density at the cathode with drift-diffusion approximation is

$$\frac{\partial n_i}{\partial t} = \nu_i n_e - \mu_i \frac{\partial n_i}{\partial z} E_{\mathrm{rf}} \cdot \cos \omega t, \tag{5}$$

where the ionization collision frequency of neutral gas $\nu_i = \alpha \cdot \mu_e E_{\mathrm{rf}} \cdot \cos \omega t$, E_{rf} is the RF electric field amplitude, n_i and n_e are the ion and electron density, and μ_i and μ_e are the ion and electron mobility, respectively. The first Townsend coefficient α is

$$\alpha = A_0 \cdot p \cdot \exp(-B_0 p / E_{\mathrm{eff}}), \tag{6}$$

where A_0 and B_0 are the constants related to the neutral gas species that are independent from pressure and electric field [13], and E_{eff} is the effective intensity of the RF field [11, 28]:

$$\begin{aligned} E_{\mathrm{eff}} &= E_{\mathrm{rf}} \cdot \frac{\nu_{eg}}{\sqrt{2}\,(\nu_{eg}{}^2 + \omega^2)^{1/2}} \\ &= \frac{V_{\mathrm{rf}}}{d} \cdot \frac{\nu_{eg0}}{\sqrt{2}\,[\nu_{eg0}{}^2 + (2\pi)^2 (f/p)^2]^{1/2}}, \end{aligned} \tag{7}$$

where $\nu_{eg0} = \nu_{eg}/p$ is the electron-neutral collision rate at the unit neutral gas pressure (e.g. 1 Torr), and we use $E_{\mathrm{rf}} = V_{\mathrm{rf}}/d$ at the early stage of breakdown neglecting the space charge effect. At the breakdown voltage, i.e., $\partial n_i/\partial t \approx 0$ [13], equation (5) becomes

$$\nu_i n_e = \mu_i \frac{\partial n_i}{\partial z} E_{\mathrm{rf}} \cdot \cos \omega t. \tag{8}$$

The continuity equation of electron density at the cathode, assuming the cylindrical discharge system, is written in the form

$$\begin{aligned} \frac{\partial n_e}{\partial t} = \nu_i n_e + D_{\mathrm{T}} \frac{1}{r} \frac{\partial}{\partial r}\left(r \frac{\partial n_e}{\partial r}\right) + D_{\mathrm{L}} \frac{\partial^2 n_e}{\partial z^2} \\ - \mu_e \frac{\partial n_e}{\partial z} E_{\mathrm{rf}} \cdot \cos \omega t + s_i + s_{\mathrm{F}}, \end{aligned} \tag{9}$$

where D_{T} is the transverse diffusion coefficient of electron, D_{L} is the longitudinal diffusion coefficient of electron, s_i is the rate of secondary electron emission induced by the ion bombardment, and s_{F} is the rate of the field emission or field-enhanced thermionic emission considering the Schottky effect with high applied electric field, i.e., thermo-field emission [29–33].

We first consider the two surface source terms. The rate of secondary electron emission governed by the ion impact is

$$\begin{aligned} s_i &= (\text{secondary emission coefficient}) \\ &\quad \times (\text{ion wall loss by the drift motion}) \\ &= \gamma \cdot \left[\mu_i \frac{\partial n_i}{\partial z} E_{\mathrm{rf}} \cdot \cos \omega t\right] = \gamma \nu_i n_e, \end{aligned} \tag{10}$$

where ion wall loss by the drift motion comes from equation (8).

For cathodes with negligible thermionic emission, the effective secondary emission coefficient [29] for the field emission, γ_{F}, can be expressed as

$$\gamma_{\mathrm{F}} = K \exp[-B/(E_{\mathrm{rf}} \cdot \cos \omega t)], \tag{11}$$

where K is the gas and material dependent constant. B is the constant from the Fowler Nordheim tunneling theory [30, 31], which depends on the work function of the material and surface irregularity. In this study, the applied DC electric field used in [29] is replaced by the applied RF field $E_{\mathrm{rf}} \cdot \cos \omega t$.

On the other hand, for cathode materials with high thermionic effect, the total field-enhanced thermionic emission current density considering the Schottky effect [32, 33] is given by

$$J_{\mathrm{F}} = A T_C{}^2 \exp(-e\varphi/k_{\mathrm{B}} T_{\mathrm{C}}) \exp\left(\sqrt{e^3 E_C / 4\pi\epsilon_0} \,/ k_{\mathrm{B}} T_{\mathrm{C}}\right), \tag{12}$$

where A is the Richardson's constant, T_{C} is the temperature of the cathode, φ is the work function of the material, k_{B} is the Boltzmann's constant, and ϵ_0 is the vacuum permittivity. The second exponential term is related to the Schottky effect which considers the field enhanced thermionic emission at the cathode. The electric field at the cathode, E_C, can be decomposed into the externally applied electric field $E_{\mathrm{rf}} \cdot \cos \omega t$ and the time-varying ion-enhanced field E^+ [29]. Assuming $E_{\mathrm{rf}} \cdot \cos \omega t / E^+ \gg 1$ we transform equation (12) to the following form

$$J_{\mathrm{F}} \approx J_E \exp\left(\sqrt{e^3 / 4\pi\epsilon_0 E_{\mathrm{rf}} \cdot \cos \omega t}\, E^+ / 2 k_{\mathrm{B}} T_{\mathrm{C}}\right), \tag{13}$$

where $J_E = A T_{\mathrm{C}}{}^2 \exp(-e\varphi/k_{\mathrm{B}} T_{\mathrm{C}}) \exp\left(\sqrt{e^3 E_{\mathrm{rf}} \cdot \cos \omega t / 4\pi\epsilon_0} / k_{\mathrm{B}} T_{\mathrm{C}}\right)$ is the thermionic emission enhanced by the external electric field. The ion-enhanced field has a power law relation with the total field emission current density [29]

$$E^{+} = CJ^{+} = CGJ_{F}{}^{n}, \tag{14}$$

where C is the constant determined by the ionic mobility and the electrode microgeometry, J^{+} is the ion current density, G is the constant attributed to the electron and ion trajectories, and n is the pressure dependent constant. Equation (13) becomes

$$J_{\mathrm{F}} = J_{E}\exp(\sqrt{e^{3}/4\pi\epsilon_{0}E_{\mathrm{rf}}\cdot\cos\omega t}\ CGJ_{\mathrm{F}}{}^{n}/2k_{\mathrm{B}}T_{\mathrm{C}}). \tag{15}$$

This transcendental equation can have a unique solution only if $\partial[J_{E}\exp(\sqrt{e^{3}/4\pi\epsilon_{0}E_{\mathrm{rf}}\cdot\cos\omega t}\,CGJ_{\mathrm{F}}{}^{n}/2k_{\mathrm{B}}T_{\mathrm{C}})\,]\big/\partial J_{\mathrm{F}}$ $=1$ [29], which yields the following relation:

$$J_{\mathrm{F}} = J_{E}\exp(1/n). \tag{16}$$

Let us define the effective thermionic emission coefficient under the high electric field as a ratio of the field-enhanced thermionic emission current density over ion current density,

$$\gamma_{\mathrm{F}} = J_{\mathrm{F}}/J^{+} = J_{\mathrm{F}}\big/GJ_{\mathrm{F}}{}^{n} = J_{E}\sqrt{e^{3}/4\pi\epsilon_{0}E_{\mathrm{rf}}\cdot\cos\omega t}\; Cn\cdot\exp(1/n)/2k_{\mathrm{B}}T_{\mathrm{C}}. \tag{17}$$

The rate of the field emission or the thermionic emission including the Schottky effect with high electric field can be written as

$$s_{\mathrm{F}} = \gamma_{\mathrm{F}}\cdot\left[\mu_{i}\frac{\partial n_{i}}{\partial z}E_{\mathrm{rf}}\cdot\ \cos\omega t\right] = \gamma_{\mathrm{F}}\nu_{i}n_{e}. \tag{18}$$

The electron density continuity equation (9) then becomes

$$\frac{\partial n_{e}}{\partial t} = (1+\gamma+\gamma_{\mathrm{F}})\nu_{i}n_{e} + D_{\mathrm{T}}\frac{1}{r}\frac{\partial}{\partial r}\left(r\frac{\partial n_{e}}{\partial r}\right) + D_{\mathrm{L}}\frac{\partial^{2}n_{e}}{\partial z^{2}} - \mu_{e}\frac{\partial n_{e}}{\partial z}E_{\mathrm{rf}}\cdot\ \cos\omega t. \tag{19}$$

The boundary conditions for $n_{e}(r, z, t)$ are

$$n_{e}(R, z, t) = 0, \tag{20}$$

$$n_{e}\left(r, \pm\frac{d}{2}, t\right) = 0. \tag{21}$$

By using the method of separation of variables, we have the following breakdown condition

$$(1+\gamma+\gamma_{\mathrm{F}})\frac{A_{0}\mu_{e0}V_{\mathrm{rf}}}{D_{\mathrm{T0}}}\cdot\exp\left(-\frac{B_{0}}{E_{\mathrm{eff}}/p}\right)pd = \left[2.405\left(\frac{d}{R}\right)\right]^{2} + \frac{D_{\mathrm{L0}}}{D_{\mathrm{T0}}}\cdot\frac{\pi^{2}}{\{1-\mu_{e0}V_{\mathrm{rf}}/[\pi(pd)^{2}(f/p)]\}^{2}}, \tag{22}$$

where $D_{\mathrm{T0}} = D_{\mathrm{T}}/p$, $D_{\mathrm{L0}} = D_{\mathrm{L}}/p$, and $\mu_{e0} = \mu_{e}/p$ are the transverse, longitudinal diffusion coefficients, and the mobility of the electron at the unit neutral gas pressure, respectively. The breakdown voltages in γ-, transition, and α-regimes comply with the following extended Paschen law,

$$V_{\mathrm{rf}} = V\left(pd, \frac{f}{p}, \gamma, \frac{d}{R}\right). \tag{23}$$

This extended Paschen law is valid unless the field or thermionic emission acts as a primary electron source because the effective field emission or field-enhanced thermionic emission coefficient, γ_{F}, depends on the electric field.

For the PIC simulation, the radius of electrodes of which area is $0.1\ \mathrm{m}^{2}$ is substantially big compared with the gap distance; thus the edge effect and d/R dependency can be ignored. The breakdown curves verifying the extended Paschen law are shown in figure 5. Figure 5(a) shows that the breakdown voltages are different with varying frequency. The breakdown curves in figure 5(b), however, overlap each other for all regimes when the driving frequency is divided by the neutral gas pressure. After reproducing the extended Paschen law of the breakdown curves using the fluid simulation [25] as shown in figure 6, the overlapping breakdown curves which show an identical tendency to that of the PIC simulations were obtained demonstrating the validity of the extended Paschen law derived from the fluid analysis.

The scaling law can be also derived from the extended Paschen law; the two overlapping breakdown curves have the same ratio of the transition frequency over the neutral gas pressure as long as they comply with the extended Paschen law conditions, i.e., $p_{1}d_{1} = p_{2}d_{2}$ and $f_{1}/p_{1} = f_{2}/p_{2}$.

$$\frac{f_{1c}}{f_{2c}} = \frac{p_{1}}{p_{2}} = \left(\frac{p_{1}}{p_{2}}\right)^{-m}\left(\frac{d_{1}}{d_{2}}\right)^{-(m+1)}. \tag{24}$$

4. Conclusions

For the micro-sized RF or microwave He plasma gas breakdown, we demonstrate that there is an abrupt breakdown transition at certain frequency, neutral gas pressure, and gap distance following the scaling law by using the single particle analysis and the PIC simulations. When the ratio, r, of the electron drift amplitude over the gap distance calculated from the single particle analysis, is bigger than 0.9, the breakdown voltage intensely depends on the secondary emission coefficient (γ-regime), whereas the secondary emission has little effect on the breakdown voltage for $r < 0.9$ (transition and α-regimes). The single particle analysis suggests that the transition frequency, f_{c}, is proportional to p^{-m} and $d^{-(m+1)}$ by using the characteristic scale method. The scaling law is well supported in the PIC simulation results. The same scaling law, however, is not corroborated in the fluid simulation results as the fluid simulation cannot fully depict the kinetic nature of the gas breakdown.

From the fluid analysis, the extended Paschen law for RF or microwave gas discharge from γ- to α-regimes is derived with the ion and electron density continuity equations. The high-frequency gas breakdown voltage can be expressed as a function of pd, f/p, γ, and d/R unless the field emission or the thermionic emission becomes dominant during the discharge process. The PIC simulations show that the extended Paschen law is valid in the frequency over neutral gas pressure domain for the same pd. The fluid simulations also validate the same extended Paschen law. The scaling law

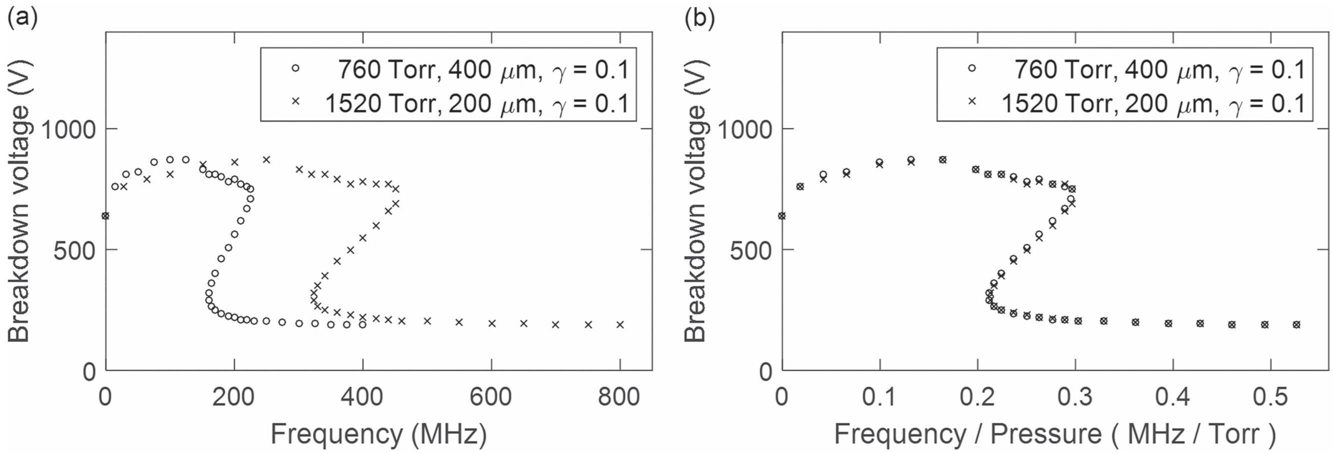

Figure 5. The PIC simulation results on breakdown curves (a) in the frequency domain and (b) showing the extended Paschen law in the frequency over the neutral gas pressure domain.

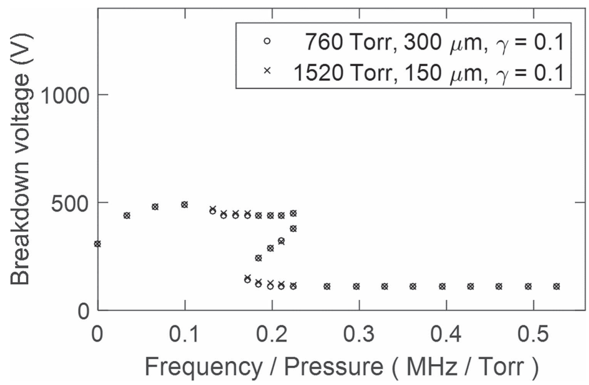

Figure 6. The fluid simulation results on the extended Paschen law of the breakdown curves in the frequency over the neutral gas pressure domain.

induced from the fluid analysis using the extended Paschen law, is identical with the law obtained from the single particle analysis and the PIC simulation.

Acknowledgments

This research was supported by the National Research Foundation of Korea under BK21 + program, grant No. 2015R1D1A1A01061556 (Ministry of Education), and grant Nos. 2015M3A9E2066986 and 2016K1A4A4A01922028 (Ministry of Science, ICT and Future Planning). This work was also partially supported by Asia-Pacific Center for Theoretical Physics.

References

[1] Schoenbach K H and Becker K 2016 20 years of microplasma research: a status report *Eur. Phys. J.* D **70** 29
[2] Schoenbach K H, Moselhy M and Shi W 2004 Self-organization in cathode boundary layer microdischarges *Plasma Sources Sci. Technol.* **13** 177–85
[3] Walsh J L and Kong M G 2007 Room-temperature atmospheric argon plasma jet sustained with submicrosecond high-voltage pulses *Appl. Phys. Lett.* **91** 221502
[4] Kang S K, Choi M Y, Koo I G, Kim P Y, Kim Y S, Kim G J, Mohamed A-A H, Collins G J and Lee J K 2011 Reactive hydroxyl radical-driven oral bacteria inactivation by radio frequency atmospheric plasma *Appl. Phys. Lett.* **98** 143702
[5] Stoffels E, Flikweert A J, Stoffels W W and Kroesen G M W 2002 Plasma needle: a non-destructive atmospheric plasma source for fine surface treatment of (bio)materials *Plasma Sources Sci. Technol.* **11** 383–8
[6] Iza F and Hopwood J A 2003 Low-power microwave plasma source based on a microstrip split-ring resonator *IEEE Trans. Plasma Sci.* **31** 782–7
[7] Choi J, Iza F, Do H J, Lee J K and Cho M H 2009 Microwave-excited atmospheric-pressure microplasmas based on a coaxial transmission line resonator *Plasma Sources Sci. Technol.* **18** 025029
[8] Kim K N, Lim J H, Yeom G Y, Lee S H and Lee J K 2006 Effect of dual frequency on the plasma characteristics in an internal linear inductively coupled plasma source *Appl. Phys. Lett.* **89** 251501
[9] Seo Y S, Lee H W, Kwon H C, Choi J, Lee S M, Woo K C, Kim K T and Lee J K 2011 A study on characterization of atmospheric pressure plasma jets according to the driving frequency for biomedical applications *Thin Solid Films* **519** 7071–8
[10] Park S J, Choi J, Park G Y, Lee S K, Cho Y, Yun J I, Jeon S M, Lee J K, Kim K T and Sim J Y 2010 Inactivation of *S. mutans* using an atmospheric plasma driven by a palm-size-integrated microwave-power module *IEEE Trans. Plasma Sci.* **38** 1956–62
[11] Herlin M A and Brown S C 1948 Breakdown of a gas microwave frequencies *Phys. Rev.* **74** 291–6
[12] Jones F L and Williams G C 1951 High-frequency discharges: I. Breakdown mechanism and similarity relationship *Proc. Phys. Soc.* B **64** 560–73
[13] Kihara T 1952 The mathematical theory of electrical discharges in gases *Rev. Mod. Phys.* **24** 45–61
[14] Lisovskiy V, Booth J-P, Landry K, Douai D, Cassagne V and Yegorenkov V 2008 Similarity law for rf breakdown *Europhys. Lett.* **82** 15001
[15] Go D B and Venkattraman A 2014 Microscale gas breakdown: ion-enhanced field emission and the modified Paschen's curve *J. Phys. D: Appl. Phys.* **47** 503001
[16] Matejčik S, Klas M, Radjenović B, Durian M, Savić M and Radmilović-Radjenović M 2013 The role of the field

emission effect in the breakdown mechanism of direct-current helium discharges in micrometer gaps *Contrib. Plasma Phys.* **53** 573–9

[17] Radmilović-Radjenović M and Lee J K 2005 Modeling of breakdown behavior in radio-frequency argon discharges with improved secondary emission model *Phys. Plasmas* **12** 063501

[18] Savić M, Radmilović-Radjenović M, Šuvakov M, Marjanović S and Petrović Z L 2011 On explanation of the double-valued paschen-like curve for RF breakdown in argon *IEEE Trans. Plasma Sci.* **39** 2556–7

[19] Korolov I and Donko Z 2015 Breakdown in hydrogen and deuterium gases in static and radio-frequency fields *Phys. Plasmas* **22** 093501

[20] Lee M U, Jeong S Y, Won I H, Sung S K, Yun G S and Lee J K 2016 Non-Maxwellian to Maxwellian transitions of atmospheric microplasmas at microwave frequencies *Phys. Plasmas* **23** 070704

[21] Phelps A V and Petrović Z L 1999 Cold-cathode discharges and breakdown in argon: surface and gas phase production of secondary electrons *Plasma Sources Sci. Technol.* **8** R21–44

[22] Hemke T, Eremin D, Mussenbrock T, Derzsi A, Donkó Z, Dittmann K, Meichsner J and Schulze J 2013 Ionization by bulk heating of electrons in capacitive radio frequency atmospheric pressure microplasmas *Plasma Sources Sci. Technol.* **22** 015012

[23] Birdsall C K 1991 Particle-in-cell charged-particle simulations, plus Monte Carlo collisions with neutral atoms, PIC-MCC *IEEE Trans. Plasma Sci.* **19** 65–85

[24] Verboncoeur J P, Langdon A B and Gladd N T 1995 An object-oriented electromagnetic PIC code *Comput. Phys. Commun.* **87** 199–211

[25] Kim H C, Iza F, Yang S S, Radmilović-Radjenović M and Lee J K 2005 Particle and fluid simulations of low-temperature plasma discharges: benchmarks and kinetic effects *J. Phys. D: Appl. Phys.* **38** R283–301

[26] Hong Y J, Yoon M, Iza F, Kim G C and Lee J K 2008 Comparison of fluid and particle-in-cell simulations on atmospheric pressure helium microdischarges *J. Phys. D: Appl. Phys.* **41** 245208

[27] Saha H P 1993 *Ab initio* calculation of scattering length and cross sections at very low energies for electron-helium scattering *Phys. Rev.* A **48** 1163–70

[28] Margenau H 1946 Conduction and dispersion of ionized gases at high frequencies *Phys. Rev.* **69** 508–13

[29] Boyle W S and Kisliuk P 1955 Departure from Paschen's law of breakdown in Gases *Phys. Rev.* **97** 255–9

[30] Fowler R H and Nordheim L 1928 Electron emission in intense electric fields *Proc. Phys. Soc.* A **119** 173–81

[31] Rumbach P and Go D B 2012 Fundamental properties of field emission-driven direct current microdischarges *J. Phys. D: Appl. Phys.* **112** 103302

[32] Herring C 1949 Thermionic emission *Rev. Mod. Phys.* **21** 187–204

[33] Sabchevski S, Illy S, Piosczyk B, Borie E and Zhelyazkov I 2008 Towards the formulation of a realistic 3D model for simulation of magnetron injection guns for gyrotrons (a preliminary study) *Wiss. Ber. FZKA* **7409** 1–34